# A novel method for thrust measurements using microparticles

**IEPC-2009-044**

*Presented at the 31st International Electric Propulsion Conference,*
*University of Michigan • Ann Arbor, Michigan • USA*
*September 20 – 24, 2009*

Viktor Schneider*, Thomas Trottenberg† and Holger Kersten‡
*Institute of Experimental and Applied Physics, University of Kiel, 24098 Kiel, Germany*

**Abstract: A novel experiment for the study of forces on microparticles in ion beams is presented. A broad beam ion source provides a vertically upward directed beam wherein hollow glass spheres with a diameter of 100 micrometer are injected. The particles are illuminated by a diode laser and recorded with a ccd camera. From the trajectories the acceleration and the net force on the particles are determined. Information on energetic neutral atoms is achieved, which is not accessible by electrostatic methods.**

## Nomenclature

| | |
|---|---|
| $a$ | = particle acceleration |
| $d, d_\mathrm{w}$ | = particle diameter and particle wall thickness |
| $e$ | = elementary charge |
| $F_\mathrm{net}, F_\mathrm{drag}, F_\mathrm{ion}$ | = net force, drag force and ion drag force acting on the particle |
| $\Phi_\mathrm{p}$ | = floating potential |
| $g$ | = gravity |
| $I_\mathrm{beam}$ | = ion source beam current |
| $I_i$ | = intensity of pixel $i$ |
| $j_\mathrm{i}$ | = measured ion current density |
| $\lambda_\mathrm{cx}$ | = mean free path for charge-exchange collisions |
| $m_\mathrm{p}, m_\mathrm{i}$ | = masses of a microparticle and an ion |
| $n_\mathrm{e}$ | = electron density |
| $r_\mathrm{p}, r_0, r_\mathrm{c}$ | = particle radius, Coulomb radius and critical parameter for impact |
| $t$ | = time |
| $U_\mathrm{anode}$ | = anode voltage |
| $v_\mathrm{i}, v_x$ | = ion velocity and particle velocity in $x$-direction |
| $W_\mathrm{i}$ | = kinetic ion energy |
| $x, x_i$ | = $x$-component of particle and pixel positions |
| $y, y_i$ | = $y$-component of particle and pixel positions |
| $x_0, y_0, t_0$ | = fit parameters |
| $z$ | = vertical distance from the ion source |

*PhD. student, Plasma Technology, schneider@physik.uni-kiel.de
†PostDoc, Plasma Technology, trottenberg@physik.uni-kiel.de
‡Professor, Plasma Technology, kersten@physik.uni-kiel.de

# I. Introduction

PRESENT-DAY space missions often require thrusters with high specific impulse in order to limit the propellant mass, e.g. for interplanetary flights and positioning of satellites. Some future missions demand very low thrust levels for drag-free positioning and attitude control, for example the Microscope mission[1] or the LISA mission.[2] The required thrusts are in the range of $\mu$N to some hundreds of mN. In the past few years some methods were developed to measure such small thrusts. Nevertheless, the conventional techniques are quite complicated and sensitive to disturbances from the environment due to the quite small thrusts to be measured.[3–5]

In this contribution we present a new experiment which stands in the context of non-conventional methods for ion beam characterization.[6] It allows spatially resolved measurements of the momentum flux density, from which the total thrust could be derived.

In a vertically upward directed ion beam with ion energies of several hundreds of eV provided by a 125 mm ECR broad beam ion source,[7] hollow glass spheres with 100 micrometer size are injected. The particles are accelerated by the gravitational force and by the momentum transfer due to the collisions between ions and particles (ion drag) and between fast neutral atoms and particles.

By stroboscopic illumination of the test particles with a diode laser and recording them with a ccd camera their trajectories are obtained. From these trajectories the acceleration and the net force on the particles are determined. First measurements with ion energies from 100 eV to 450 eV show a force acting on a single test particle in the order of $10^{-10}$ N.

# II. Experimental Setup

The stainless steel vacuum chamber (Fig. 1) is basically a cylinder with an inner diameter of 30 cm and a height of 40 cm. It is closed at the top with a convex cover, which has flanges for the dust injector and the particle diagnostic. A lateral 15 cm wide crosspiece is used for mounting the turbomolecular pump and provides a port for optional probe diagnostics. The ion source is attached to the lower flange of the vacuum chamber, so that the ion beam is vertically upwards directed. In the following the components are described in detail.

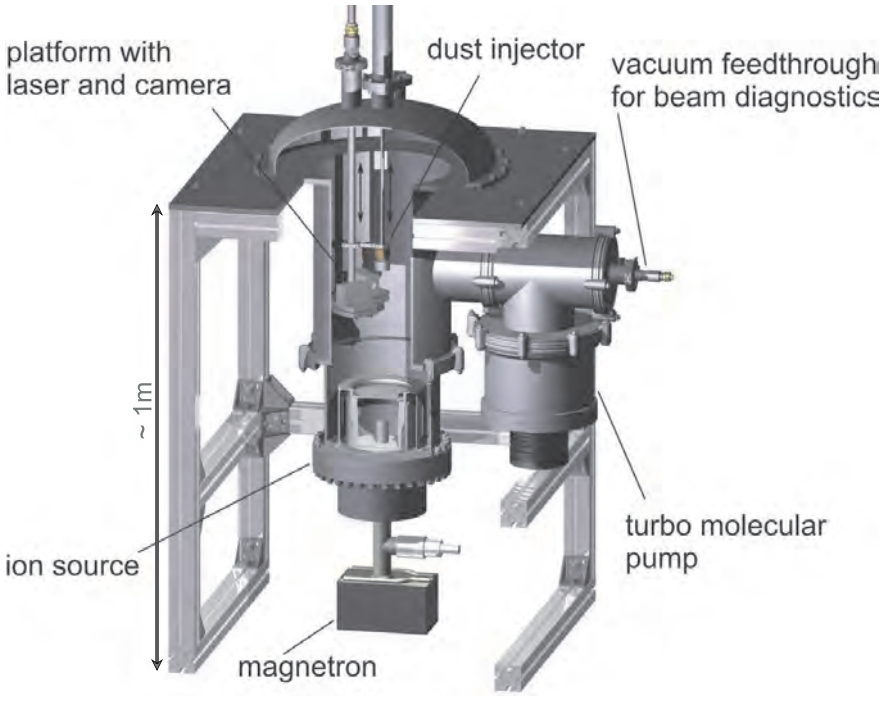


**Figure 1. Schematic side view of the setup. The upwards directed ion source provides a vertically oriented ion beam in which particles are injected. Dust injector and observation platform can be positioned independently on the vertical axis.**

### A. Ion Source

The ion beam is produced by a broad beam ion source, which has been designed for industrial use (Ion-Tech® MW/A 125 from Ion-Tech GmbH, Germany). The performance of this source has been investigated earlier and can be found in.[7] The source uses electron cyclotron resonance (ECR) in a microwave field for ionization of the process gas argon. The pressure in the vacuum chamber is $5 \cdot 10^{-2}$ Pa and somewhat higher in the source chamber, where the gas flows in. A quarter-wavelength long stub antenna emits 2.4 GHz microwaves (approximately 360 W) through a quartz cup, which separates atmospheric from vacuum pressure, into the discharge chamber. Permanent magnets provide the magnetic field for the electron resonance, which occurs at 87.5 mT in two toroidal regions around the antenna. Two planar molybdenum grids with a diameter of 125 mm and 751 circular 3.2 mm holes are used for extraction and acceleration of the ions. The ion energy is chosen by means of the voltage $U_{\mathrm{anode}}$ of an anode ring in the ceramic chamber, which allows to shift the plasma potential (approximately 60 V above the anode potential) to corresponding positive potentials. The ions are accelerated by the potential difference between the floating inner (screen) grid and the outer (accelerator) grid. However, the actual ion energy is essentially determined by the potential difference between the source plasma and the local potential in the target chamber. The ion source produces beam currents up to $I_{\mathrm{beam}} \approx 120$ mA. While the screen grid is floating, the accelerator grid can be biased negatively (up to $-1000$ V) in order to optimize the ion trajectories with respect to the losses due to ions striking the accelerator grid and is set to $-300$ V throughout this paper.

### B. Probe particles and their injection

The test particles are differentially sieved 3M ™ K1 hollow glass spheres with a size distribution of $d = (99.4 \pm 13.4)$ $\mu$m. To obtain these sizes the raw material, which contains particles from 5 to 120 $\mu$m, was sieved with a stack of two framed sieves. The upper and lower sieves had mesh widths of 112 $\mu$m and 90 $\mu$m, respectively. Additionally, but still not applied in the experiments described in this paper, the air below the lower sieve can be extracted by a pump which provides an air stream through both sieves allowing a faster separation of the desired sizes between the two sieves. For removal of broken glass spheres, the material was washed with isopropanol, so that the faultless spheres floated and could be collected from the surface, whereas the fragments sedimented to the bottom. The residual alcohol between the particles evaporated eventually. The resulting narrowed distribution is shown in Fig. 2(a). The calculated particle mass was $m_{\mathrm{p}} = (5.0 \pm 2.3) \cdot 10^{-11}$ kg with a wall thickness of $d_{\mathrm{w}} = (0.74 \pm 0.28)$ $\mu$m determined from scanning electron microscope images of intentionally crushed particles (see Fig. 2(b)).

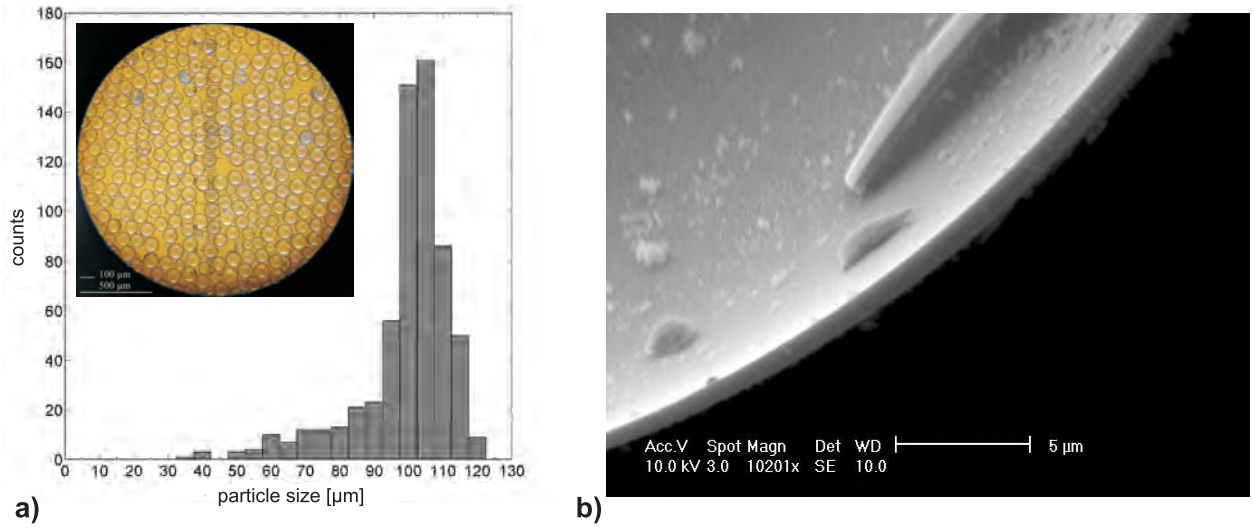


**Figure 2. a) Particle size distribution and conventional light microscope image of the glass spheres. b) Scanning electron microscope image of a crushed particle for the determination of the wall thickness and the particle mass.**

The dust injecting device is a small container with 300 $\mu$m opening which is vertically shaken by an electromagnet with an amplitude $< 1$ mm (see Fig. 3). It injects with every pulse some particles with a

nearly vertical initial velocity into the vacuum chamber. The dust injector can be moved vertically along the common axis of the vacuum chamber and the ion source, which allows an injection at different positions in the ion beam.

### C. Particle observation

The injected particles are observed by recording their 90-degrees-scattered laser light from a 5 mW horizontally oriented laser diode (655 nm), which is vertically expanded to a thin fan (< 1 mm). The laser and the charge-coupled device (ccd) camera are mounted on a translation platform (see Fig. 3), which allows particle tracking at different distances from the ion source. Camera and laser are shielded by metal boxes with thin glass windows from the beam generated secondary plasma, but are exposed to the vacuum, which is not a disadvantage because their electronic components do not contain volatile substances. The platform is water-cooled in order to protect camera and laser from the heat produced by the impinging ions at the bottom side. Figure 3(a) shows the sandwich design with two steel plates and a water pipe in between. The heat conduction from the lower plate, which serves as heat shield, through the pipe to the upper plate is efficiently interrupted by the cooling water, so that the measured temperature in the boxes does not exceed 50 °C.

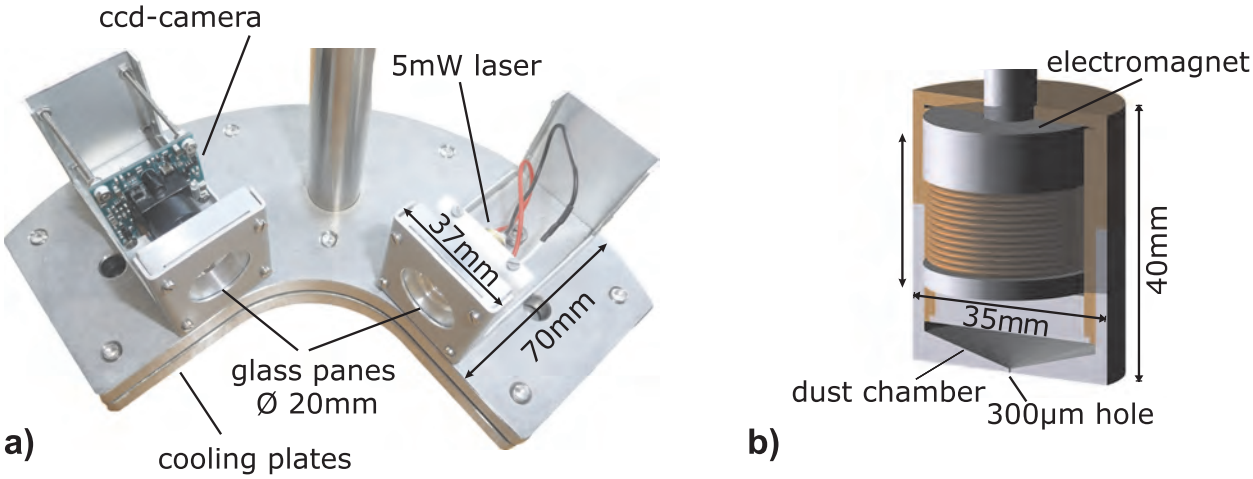


**Figure 3. Translation platform for particle tracking (a) and the dust injector (b). The electronic components are exposed to the vacuum and shielded from the heat produced by the ion beam by a sandwich design of two steel plates with water-cooling in between.**

The 1/3 inch ccd camera has a resolution of 510 × 492 pixels and provides a composite video signal with 25 frames per second. It is equipped with a $f = 6$ mm lens and interference filter at the laser wavelength in order to suppress light from the secondary plasma and stray light from the ion source. The camera lens is focussed on the illuminated volume and has a field of view of 38.8 mm × 29.1 mm. The laser is pulsed with frequencies ranging typically from 300 to 1000 Hz for stroboscopic illumination of the falling particles.

## III. Data Acquisition and analysis

A framegrabber digitizes the analog signal and extracts single frames from the video. The images are distorted due to the small focal length ("fisheye lens"). To obtain real coordinates for a measured pixel position, we used a reference chart with vertical and horizontal lines in the focal plane to determine the real coordinates of the lines' pixel positions, and interpolated linearly for all pixels. The frame is then resampled to an undistorted image by means of bicubic convolution interpolation.[8] The resulting resolution is 40.46 $\mu$m/pixel.

The stroboscopic illumination of the particles results in trajectories with particle positions displayed as dots. Every dot covers several pixels $i$ with different intensity values $I_i$. Using these intensities and the coordinates of each pixel $(X_i, Y_i)$ yields a subpixel resolution for the particle position $(x, y)$ in each direction:

$$x = \frac{\sum X_i I_i}{\sum I_i} \quad , \quad y = \frac{\sum Y_i I_i}{\sum I_i} \tag{1}$$

Since the time for a particle to transit the field of view is comparable to the frame period, one trajectory typically extends over two consecutive frames. The trajectory of a free falling particle shown in Fig. 4(a), for instance, was reassembled from two frames. Due to the stroboscopic illumination with 500 Hz, each spot serves as timestamp.

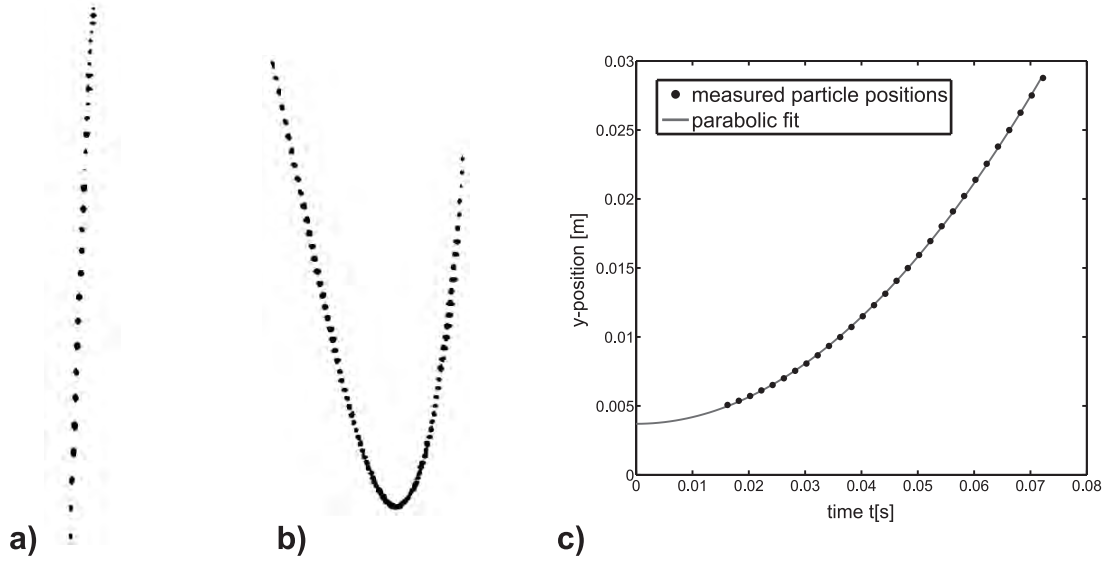


**Figure 4. Particle trajectories (a) of a free falling particle and (b) with a 410 eV beam. The stroboscopic frequency is 500 Hz in both cases. (c) Measured particle positions of the trajectory shown in (a) and the parabolic fit from Eq. (2).**

With $x$ and $y$ denoting the horizontal and vertical position, the motion can than be described as

$$\vec{s}(t) = \begin{pmatrix} x(t) \\ y(t) \end{pmatrix} = \begin{pmatrix} v_x t + x_0 \\ \frac{1}{2} a (t - t_0)^2 + y_0 \end{pmatrix} \quad , \tag{2}$$

where $t$ denotes the time, and the constants with index zero as well as the velocity $v_x$ and the acceleration $a$ are fit parameters. For a set of equally spaced time values $t_i$ corresponding to the laser pulse frequency, the resulting set of y-positions $y(t_i)$ reproduces well the dotted trajectory (see Fig. 4(c)).

Figure 4(b) shows another particle trajectory with a particle exposed to the ion beam. It is injected into the field of view with an initial, essentially downward directed velocity, decelerates, reaches a turning point and is accelerated upwards. The trajectory is a parabola and indicates, that the movement has a constant horizontal velocity $v_x$ and a uniform vertical acceleration $a$.

In the next step, the drag force can be deduced from the measured acceleration $a$. The net force in vertical direction $F_{\mathrm{net}} = m_{\mathrm{p}} a$ is the superposition of gravitational force $m_{\mathrm{p}} g$ and drag force $F_{\mathrm{drag}}$. Since these are opposed to each other, the absolute value of the drag force is

$$F_{\mathrm{drag}} = m_{\mathrm{p}}(a - g) \quad . \tag{3}$$

## IV. Measurements and Discussion

With the new experiment two first measurements were performed. In the first one the dust injecting device was located at the upper edge of the field of view and was raised 5 cm for the second measurement. The position of the translation platform was 30 cm above the ion source in both series of measurements. The trajectories of the accelerated particles were recorded for each position and for ion beam energies up to $\sim 500$ eV. Figure 5 shows the forces acting on the particles for different ion energies obtained from about three thousand trajectories ($\triangle, \triangledown$), and the error bars indicate the standard deviation. As expected, the net

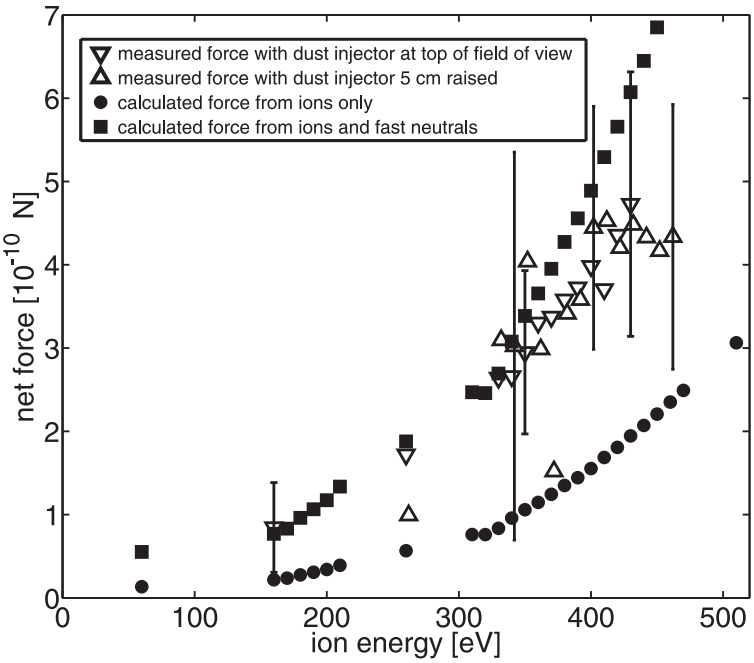


**Figure 5. Measured net forces on the test particles and calculated forces due to ions and fast neutrals based on the ion beam current measurements.**

force increases with higher ion energies up to $\sim 4.5{\cdot}10^{-10}$ N, which is comparable with the gravitational force. This is in a good agreement with our measurements, where above 500 eV no particles left the injector. Also, the forces in both measurements are in good agreement, which indicates that the dust dispenser position has no disturbing influence on the ion beam and the momentum transfer, respectively.

These measurements can be compared with the calculated ion drag force based on a beam current density measurement with a Faraday cup. The cup has a circular collector plate (diameter 8 mm) behind a negatively biased grid (−20 V, transparency 40%) to impede electrons from the target chamber and to avoid escaping secondary electrons created at the collector.

We expect that the particle surface potential (floating potential) is much lower than the potential $W_\mathrm{i}/e$ up to which ions with kinetic energy $W_\mathrm{i} = \frac{1}{2} m_\mathrm{i} v_\mathrm{i}^2$ would charge the particle without any discharging mechanism. A measurement with a floating cylindrical Langmuir probe in the observation volume yields floating potentials of only $+2 \ldots +3$ V. This finding can be attributed to discharging with electrons, which are produced by collisions of the ions with the walls and neutral gas. In our setup an electron density of $n_\mathrm{e} \approx 10^{14}$ m$^{-3}$ was measured with Langmuir probes, which is sufficient to balance the ion current due to the beam at a potential of $\Phi_p \approx +2$ V (orbital motion limited theory[9]). Significant discharging by electrons was also observed by Svestka *et. al.* in the microparticle charging experiments with energetic ion beams in a quadrupole trap.[10]

An important parameter for Coulomb scattering is the Coulomb radius

$$r_0 = (e\Phi_p / m_\mathrm{i} v_\mathrm{i}^2) r_\mathrm{p} \qquad , \tag{4}$$

which is defined as the impact parameter for 90-degrees scattering. In our case is therefore $r_0 \ll r_\mathrm{p}$, indicating that either an ion is Coulomb scattered with very small angle or it reaches the surface. The critical parameter for impact $r_\mathrm{c} = r_\mathrm{p}(1 - (2r_0/r_\mathrm{p}))^{1/2}$ is, for the same reason, nearly identical with the geometrical radius, $r_\mathrm{c} \approx r_\mathrm{p}$.

Therefore, we can use the geometrical cross section to calculate the ion drag force $F_\mathrm{ion}$ as a function of the measured ion current densities $j_\mathrm{i}$ and the preset ion energy $W_\mathrm{i}$, assuming that the impinging ions transfer their entire momentum to the microparticle:

$$F_\mathrm{ion} = \pi r_\mathrm{p}^2 \frac{j_\mathrm{i}}{e} \sqrt{2 W_\mathrm{i} m_\mathrm{i}} \qquad . \tag{5}$$

In comparison with the calculated force (●) from the beam current measurements (see Eq.(5)) the net force is much higher. This can be explained by the momentum transfer due to fast neutrals, which are not

detected with a Faraday cup. At energies above 100 eV charge-exchange collisions between the beam ions and the neutral gas are the dominating process and the collision cross sections are energy dependent.[11] In an $Ar^+ + Ar$ charge-exchange collision the ion is converted into a fast neutral atom without significant change of speed and direction. The corresponding mean free paths are in the range of $\lambda_{cx} = (25 \pm 3)$ cm. This means, that at a distance of $z = 30$ cm only $\exp(-z/\lambda_{cx}) = (30 \pm 5)\%$ of the argon beam is still ionized so that the ion drag force is only this fraction of the total drag force. The calculation of the total force produced by the sum of ions and fast neutrals is also shown in Fig. 5 (■), and is in a good agreement with the measured results.

## V. Conclusion

In this paper we introduced a novel experiment for the measurement of forces on microparticles in ion beams. With the configuration of a ccd camera and a laser operated in the ion beam, it is possible to record particle trajectories, from which the acceleration and the total force acting on the microparticles are obtained. First measurements with the new technique show results which, compared with the calculated forces from ion beam current measurements, indicate, that more than the half of the force is caused by fast neutral atoms in the ion beam which are produced by charge-exchange collisions.

The development and testing of ion thrusters requires sophisticated beam diagnostics and thrust measurements. The described method can be a useful extension for space-resolved force measurements and non-electrostatic beam diagnostics. Additionally, the total thrust could be determined by integrating the spatially measured momentum flux density over the whole beam profile.

## Acknowledgments

The technical assistance of Michael Poser and Volker Rohwer is gratefully acknowledged.

## References

[1]Touboul, P., Rodrigues, M., Mtris, G., and Tatry, B., "MICROSCOPE, testing the equivalence principle in space," *C. R. Acad. Sci. Paris*, Vol. 2, No. 9, 2001, pp. 1271–1286.

[2]Danzmann, K. and The LISA Study Team, "LISA - An ESA Cornerstone Mission for the Detection and Observation of Gravitation Waves," *Adv. Space Res.*, Vol. 32, No. 7, 2003, pp. 1233–1242.

[3]Rocca, S., Menon, C., and Nicolini, D., "FEEP micro-thrust balance characterization and testing," *Meas. Sci. Technol.*, Vol. 17, 2006, pp. 711–718.

[4]Packan, D., Bonnet, J., and Rocca, S., "Thrust Measurements with the ONERA Micronewton Balance," *IEPC*, No. 118, The 30th International Electric Propulsion Conference, Florence, Italy, 2007, pp. 1–13.

[5]Gessini, P., Sandonato, G. M., Irita, R. T., Gonalves, J. A. N., and Fernandes, G. F., "A Pendulum Target Balance for Ion Engine Thrust Measurement," *IEPC*, No. 149, The 30th International Electric Propulsion Conference, Florence, Italy, 2007, pp. 1–12.

[6]Kersten, H., Wiese, R., Neumann, H., and Hippler, R., "Interaction of ion beams with dusty plasmas," *Plasma Phys. Control. Fusion*, Vol. 48, 2006, pp. B105–B113.

[7]Zeuner, M., Scholze, F., Neumann, H., Chassé, T., Otto, G., Roth, D., Hellmich, A., and Ocker, B., "A unique ECR broad beam source for thin film processing," *Surface and Coatings Technology*, Vol. 142-144, 2001, pp. 11–20.

[8]Keys, R. G., "Cubic Convolution Interpolation for Digital Image Processing," *IEEE Transactions on Acoustics, Speech, and Signal Processing*, Vol. ASSP-29, No. 6, 1981, pp. 1153–1160.

[9]Mott-Smith, H. M. and Langmuir, I., "The theory of collectors in gaseous discharges," *Physical Review*, Vol. 28, 1926, pp. 727–763.

[10]Svestka, J., Cermak, I., and Grün, E., "Electric Charging and Electrostatic Fragmentation of Dust Particles in Laboratory," *Adv. Space Res.*, Vol. 13, No. 10, 1993, pp. 199 – 202.

[11]Phelps, A. V., "The application of scattering cross sections to ion flux models in discharge sheaths," *J. Appl. Phys.*, Vol. 76, No. 2, 1994, pp. 747–753.